DOI: https://doi.org/10.15276/hait.09.2026.41
UDC 621.396.67:621.391:004.89

Model-based sensitivity analysis of dual-channel software-defined radio direction finding for unmanned aerial vehicle control signals

Serhii V. Zabolotnii[1), 3)]
ORCID: https://orcid.org/0000-0003-0242-2234; zabolotnii.serhii@csbc.edu.ua. Scopus Author ID: 56352587900
Anatolii V. Chepynoha[2)]
ORCID: https://orcid.org/0000-0003-3921-6557; a.chepynoha@chdtu.edu.ua. Scopus Author ID: 57222273315
Pavlo A. Klopotovskyi[2)]
ORCID: https://orcid.org/0000-0002-4958-2377; p.klopotovskyi@chdtu.edu.ua. Scopus Author ID: 60633744900
Vitalii V. Koval[3)]
ORCID: https://orcid.org/0000-0003-0158-4872; vitkoval@ukr.net
[1)] Cherkasy State Business College, 243, Chornovola Str. Cherkasy, 18028, Ukraine
[2)] Cherkasy State Technological University, 460, Shevchenka Bulv. Cherkasy, 18006, Ukraine
[3)] State Scientific Research Institute of Armament and Military Equipment Testing and Certification, Cherkasy, Ukraine

ABSTRACT

Relevance. Direction finding of drone-control emissions supports spectrum monitoring when protocol identifiers are unavailable, but open datasets provide neither phase-coherent dual-channel captures nor independent devices. **Aim.** This study evaluates whether a reproducible radio-frequency gate followed by an amplitude-comparison direction-finding proxy is internally consistent under an explicit two-channel antenna model and identifies the assumptions that bound its use. **Objectives.** The work separates tuning from final evaluation and examines conditioning, calibration, multipath, and negative-class composition without constructing an unsupported total error budget. **Methods.** Single-channel in-phase/quadrature Tampere recordings feed burst detection and fingerprinting; the second channel and directional responses are simulated. Complete recordings are divided chronologically into train, validation, and untouched test blocks with guard intervals. The threshold is selected only on validation data. Test rates receive Wilson confidence intervals, and the receiver-operating-characteristic area uses a stratified bootstrap. A circular moving-block bootstrap supplies the median interval used by the null detector. Multipath sensitivity is summarized over independent nuisance draws at each model point. **Scientific novelty.** The contribution is reproducible integration with falsifiable boundaries: sufficient differential-response slope and absence of saturation define the well-conditioned set, while fingerprint claims are tied to recording and negative-class coverage. **Practical significance.** The workflow prevents test-threshold leakage and supplies calibration and conditioning checks before hardware trials. **Results.** On the untouched within-recording test block, the validation-selected threshold yielded high precision and recall, but the pre-specified precision criterion was not met. All matched-model proxy scenarios and all angles of the independent acceptance sweep passed the software checks; neither result is a field-accuracy estimate. The edges of the angular sector were excluded from the well-conditioned set because one channel saturates there and the local slope vanishes. **Conclusions.** The pipeline is computationally coherent under its model, whereas cross-device recognition, field-clutter performance, and joint field accuracy remain unverified. Independent sessions, field-relevant negatives, antenna calibration, and live coherent two-channel measurements are required.

Keywords: Software-defined radio; direction finding; radio-frequency fingerprinting; amplitude comparison; dependent-data bootstrap; unmanned aircraft system

***For citation*: Zabolotnii S. V., Chepynoha A. V., Klopotovskyi P. A., Koval V. V. "Model-based sensitivity analysis of dual-channel software-defined radio direction finding for unmanned aerial vehicle control signals". *Herald of Advanced Information Technology*. 2026; Vol.9 No.4: 671–682. DOI: https://doi.org/10.15276/hait.09.2026.41**

INTRODUCTION

Passive radio-frequency monitoring is an important component of the detection and localization of unmanned aerial vehicles when optical or acoustic channels are unreliable. For direction finding of the control transmitter, it is not sufficient to merely detect activity within the frequency band: prior to angle estimation, it is necessary to select only those packets that belong to the target transmitter.

© Zabolotnii S., Chepynoha A., Koval V., Klopotovskyi P., 2026

The open Tampere/Zenodo datasets [1] provide real single-channel signals of DJI and other drone controllers, but do not include live dual-channel reception with known antenna geometry.

Furthermore, a stable OcuSync packet identifier could not be extracted from open header analysis without reverse engineering. Therefore, an architectural decision was made: target burst packets are selected not by a protocol-level identifier, but by radio-frequency fingerprinting [2], [3], [4], after which they are passed through a software-based prototype of a dual-channel amplitude direction finder.The contribution of this paper is twofold. First, it presents a reproducible integration of a

This is an open access article under the CC BY license (https://creativecommons.org/licenses/by/4.0/deed.uk)

streaming packet detector, a radio-frequency fingerprint gate, a dual-channel directional-response simulator, a differential-amplitude estimator, dependent-data uncertainty estimation, a null detector, and angle inversion. Second, it defines falsifiable applicability boundaries for the integrated chain under explicit open-data and antenna-model assumptions. The individual algorithms are established; the contribution is their auditable integration and model-based sensitivity analysis.

This framing deliberately separates software-consistency checks from empirical accuracy claims. The study evaluates threshold leakage, response conditioning, antenna-calibration mismatch, Monte Carlo multipath sensitivity, classifier choice, and conditional prior shift. These separate axes are not summed into a total error budget because a defensible joint distribution of nuisance parameters is unavailable.

LITERATURE REVIEW AND PROBLEM STATEMENT

Prior work on radio-frequency fingerprinting for unmanned system identification has demonstrated that physical signal features can distinguish UAV controllers from Wi-Fi/Bluetooth interference [2] and support hierarchical detection and identification of UAVs [3], although the generalization of such fingerprints across devices and environments remains an open problem [4]. Contemporary approaches based on learning from radio data (RadioML) provide a broader context for automatic radio signal classification, while the problem of transferring such models across environments has been systematized in a survey on transfer learning for RadioML [5]. In our formulation, fingerprint-based identification is not an end goal but a gating module that replaces the unavailable protocol-level identifier.

The field of SDR-based drone monitoring encompasses the detection of frequency-hopping spread spectrum (FHSS) signals, wideband spectrum scanning, and the integration of signal detection, identification, and direction-of-arrival (DOA) estimation [6–8]. These studies confirm the practical viability of the SDR approach; however, they do not bridge the gap between real single-channel signals and the absence of a live dual-channel antenna response in open datasets.

DOA estimation methods can be organized according to their angular resolution and implementation cost. High-resolution antenna-array approaches, such as MUSIC and Capon minimum-variance beamforming, reviewed in [9], provide superior resolution but require a coherent multichannel array and precise calibration. Classical radar monopulse techniques [10] and amplitude-comparison methods [11] remain practical when only a limited number of channels are available; recent studies have further refined ambiguity resolution for amplitude-comparison direction finding [12].

For drone signals, direction-of-arrival estimation has been investigated with a switched-beam antenna and a single-channel receiver [13], on small-unmanned-aircraft platforms [14], and using multimode antennas [15]. The present study instead considers an amplitude-comparison proxy and therefore follows conditioning and calibration concepts from monopulse estimation [10–12]. Because the rolling statistic is a median of dependent observations, its interval is estimated by the moving-block bootstrap for stationary observations [16], rather than by a mean-oriented heteroskedasticity-and-autocorrelation-consistent standard error. Spectral features use standard periodogram estimates, and propagation sensitivity uses two-ray and Rayleigh models [17].

The non-Gaussian component of the processing chain is associated with reconstruction features in the Kunchenko space and polynomial estimation methods [18–21]. In the present work, these concepts are employed in a limited role: fractional real and imaginary DSGE descriptors are incorporated into the radio-frequency fingerprint vector alongside spectral samples.

RESEARCH AIM AND OBJECTIVES

The aim of this study is to evaluate an open software concept of a dual-channel software-defined-radio processing chain for amplitude-comparison direction finding of DJI Mavic signals and to determine its model-dependent applicability under the limitations of public single-channel recordings.

The following tasks are defined to achieve the aim of the study:

1. To establish a validation boundary using open recordings while explicitly distinguishing held-out time blocks from independent sessions or devices.
2. To verify a fallback (Plan B) target selection pathway after unsuccessful OcuSync header analysis.
3. To construct a processing pipeline consisting of packet detection, radio-frequency fingerprint selection, dual-channel simulation, differential amplitude, moving-block-bootstrap aggregation, null detection, and inverse angle recovery.

ISSN 2663-0176 (Print)
ISSN 2663-7731 (Online)

4. To report every numerical result directly from the generated data artifacts of the fingerprinting, evaluation, and simulation procedures - without manual rounding outside the tables - so that all reported figures are fully reproducible.

5. To characterize response conditioning, antenna-calibration mismatch, Monte Carlo multipath sensitivity, and conditional class-prior shift as separate sensitivity axes.

6. To analyze the sensitivity of the gating module to feature groups and classifier choice without inferring field readiness from within-recording results.

7. To explicitly separate evidence of processing-chain consistency from claims regarding field accuracy.

MATERIALS AND METHODS

The signal source is the Tampere/Zenodo dataset "Radio-Frequency Control and Video Signal Recordings of Drones" (DOI: 10.5281/zenodo.4264467) [1]. The 2.44 GHz files contain int16 interleaved in-phase/quadrature samples at 120 MS/s. One recording is available per controller class; therefore, cross-device and cross-session generalization cannot be tested. Windows are sampled across each complete recording and split chronologically into training (2975 windows), validation (950), and untouched test (975) blocks, with five-window guard intervals at both boundaries. Model selection and the full-precision threshold are fixed on validation data before the test block is scored once (Table 1).

The processing-chain architecture is shown in Fig. 1. The diagram explicitly separates the inaccessible OcuSync protocol pathway, the fallback (Plan B) RF fingerprint-based selection pathway, and the regions corresponding to real single-channel I/Q data versus the simulated dual-channel response.

The complete implementation of all pipeline modules, the exact configuration, the trained fingerprint model, and the result artifacts underlying every table and figure are openly available in the public code supplement repository (https://github.com/SZabolotnii/SDR_POC_Pelengator-code-supplement).

The simulation configuration is presented in Table 2. Each channel uses a cosine-squared power pattern with normalized beam coordinate $u_i = (\theta - \varphi_i)\pi / (2BW_3)$. The measured amplitude ratio and the equivalent simulated power-gain ratio are kept distinct; their equality follows because the simulator applies the square root of power gain to signal amplitude.

$$G_i(\theta) = max\{cos^2 u_i, \varepsilon\}. \quad (1)$$

Table 1. **Modules of the proposed processing pipeline**

Module	Input	Output	Role
Packet detector	I/Q stream	Burst intervals	Schmitt-trigger detection on a smoothed log-power envelope
Header inspection	Burst bytes	Plan-B decision	Negative result for a stable public OcuSync identifier
Fingerprint filter	Burst I/Q windows	Target probability	DSGE/spectral Mavic-versus-rest gate
Dual-channel simulator	Single-channel burst and angle	Two simulated channels	Directional antenna proxy with noise and multipath
Differential amplitude	Two channels	Amplitude difference	20 $\log_{10}$ amplitude observable in decibels
Rolling/bootstrap module	Burst-wise differences	Median and 95% interval	Robust aggregation and dependent-data uncertainty
Null detector	Rolling median interval	Null event	Near-balanced response using corrected uncertainty
Angle inversion	Final amplitude difference	Angle estimate	Grid-search inversion within model boundaries

Source: **compiled by the authors**

In Eq. (1), $i \in \{A, B\}$ identifies the receiving channel; θ is a signal angle of arrival; φ_i is a boresight angle of channel i; BW_3 is a full 3-dB beamwidth; u_i is a normalized beam coordinate defined above; $G_i(\theta)$ is a channel power gain on a linear scale; and $\varepsilon = 10^{-6}$ is a linear gain floor corresponding to −60 dB. The angles θ, φ_i, and BW_3 are expressed in the same angular units (degrees in this study).

$$\Delta dB = 20log_{10}(A/B) = 10log_{10}(GA/GB). \quad (2)$$

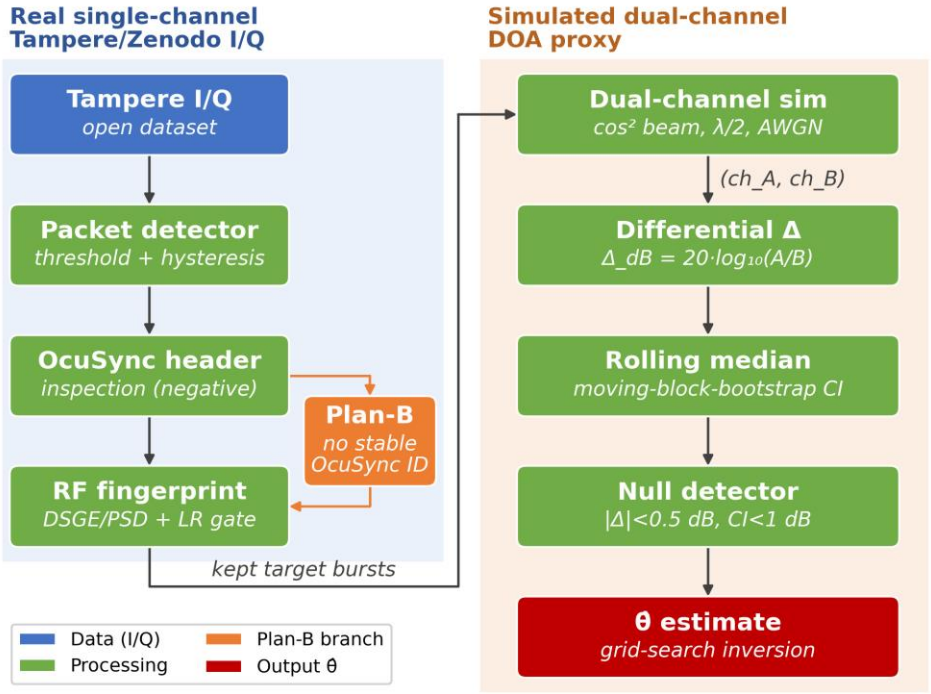


Fig. 1. **Pipeline of the dual-channel direction-finding proxy**

Source: **compiled by the authors**

Table 2. **End-to-end proxy configuration**

Parameter	Value
Sampling rate	120.0 MS/s
Target angles	−45, 0, +30, +60 degrees
Antenna boresights	+30 and −30 degrees
Beamwidth at 3 dB	60 degrees
Antenna phase-center spacing	0.0625 m (approximately λ/2 at 2.412 GHz)
Carrier frequency in proxy	2.412 GHz
Pattern floor	−60 dB
Signal-to-noise ratio	10 dB
Multipath taps in proxy	None (separate Monte Carlo study)
Rolling window	25 bursts
Median interval	Circular moving-block bootstrap: block 6, 2,000 replicates
Acceptance tolerance	5 degrees (consistency check only)

Source: **compiled by the authors**

In Eq. (2), A and B are the per-burst amplitude estimates, computed as the mean magnitude of the complex I/Q samples in channels A and B, respectively; G for channels A and B denotes the corresponding linear power gains; ΔdB is the differential amplitude in decibels; and $\log_{10}$ denotes the base-10 logarithm.

The forward simulator and inverse estimator share the same cosine-squared pattern, so the matched mapping is exact by construction and is treated only as a software-consistency check. The rolling estimate is the median of the latest 25 burst-wise differences. Its 95% interval is obtained from 2,000 circular moving-block-bootstrap replicates with block length six, and the null detector uses this median interval directly.

$$\Delta = median(\Delta),\ CI_{95} = Q_{2.5,97.5}(\Delta^*). \qquad (3)$$

In Eq. (3), Δ_j is a burst-wise differential amplitude for burst j; n = 25 is a rolling-window length; $\tilde{\Delta}$ is a sample median of the n most recent differences; Δ^* denotes a median obtained from one circular moving-block bootstrap resample; $Q_{2.5,97.5}$ denotes the 2.5th and 97.5th percentiles over 2,000 bootstrap medians; and CI_{95} is a resulting percentile 95% confidence interval. The bootstrap block length is six bursts.

(I) Conditioning: angle inversion minimizes the difference between the observed and modeled differential response. The well-conditioned set requires both an absolute local slope of at least 0.30 dB/degree and absence of channel saturation; consequently, ±30° are excluded rather than treated as valid endpoints.

$$\theta = argmin\left|\Delta(\theta) - \Delta\right|,\ \theta \in W\ . \qquad (4)$$

In Eq. (4), $\hat{\theta}$ is the estimated angle of arrival; is the modeled differential response at candidate angle θ; Δ is the measured rolling median from Eq. (3); arg min selects the angle that minimizes the absolute mismatch; and W is the well-conditioned search set in which $|d\Delta / d\theta| \geq 0.3$ dB/degree and neither channel is saturated at the pattern floor.

(II) Calibration model mismatch: the forward Δ is generated using the true geometry, while the inverse model is computed under perturbed assumptions (beamwidth error, boresight shift, and gain imbalance), resulting in realistic errors in $\hat{\theta}$.

(III) Multipath sensitivity: two-ray and six-tap Rayleigh conditions are evaluated with 100 independent draws of phases, delays, arrival angles, tap gains, and additive-noise seeds at every angle and power level. Median absolute error, empirical 95% intervals, and the fraction exceeding 5° are reported; no single fixed tap realization is interpreted as a distribution.

(IV) Field-prior adaptation: precision at a hypothetical target prevalence is computed from within-recording TPR and FPR only as a conditional scenario (Eq. (5)). Wi-Fi, Bluetooth, and background/clutter negatives are absent, so transfer of those rates to the field is unverified.

$$PPV(\pi) = \pi TPR / \left[\pi TPR + (1-\pi) FPR\right] \quad (5)$$

In Eq. (5), $PPV(\pi)$ is a positive predictive value (precision) at assumed target prevalence $\pi = P(Y=1)$; $TPR = P(+|Y=1)$ is a true-positive rate; $FPR = P(+|Y=0)$ is the false-positive rate; $Y=1$ denotes a target (DJI Mavic) burst; and + denotes a positive decision by the fingerprint gate.

(V) Gating-classifier sensitivity: logistic regression, random forest, and radial-basis-function support-vector machines use the same chronological partitions. Each operating threshold is selected on validation data and evaluated once on the untouched test block.

RESEARCH RESULTS

At the fingerprinting stage, the 19-feature vector comprises four fractional real/imaginary DSGE descriptors and 15 log-PSD samples. On the corrected chronological split, the full logistic model achieved ROC AUC 0.9855, precision 0.9378, and recall 0.9282 on the untouched test block (Table 3). The displayed validation-selected threshold was 0.181766; its full value is stored in the JSON artifact. Ablation yielded AUC 0.9855 for the full vector, 0.9855 for PSD-only, and 0.5070 for DSGE-only. These are within-recording results from one source file per class and do not demonstrate cross-device generalization.

Table 3. **Fingerprint filter metrics**

Metric	Untouched test result
Train / validation / test	2975 / 950 / 975 windows
Validation-selected threshold	0.181766 (full value stored in JSON)
TP / FP / TN / FN	181 / 12 / 768 / 14
Precision (95% CI)	0.9378 [0.8945, 0.9641]
Recall/TPR (95% CI)	0.9282 [0.8831, 0.9568]
FPR (95% CI)	0.0154 [0.0088, 0.0267]
ROC AUC (95% CI)	0.9855 [0.9722, 0.9949]
Precision ≥0.95 criterion	FAIL; within-recording result only

Source: **compiled by the authors**

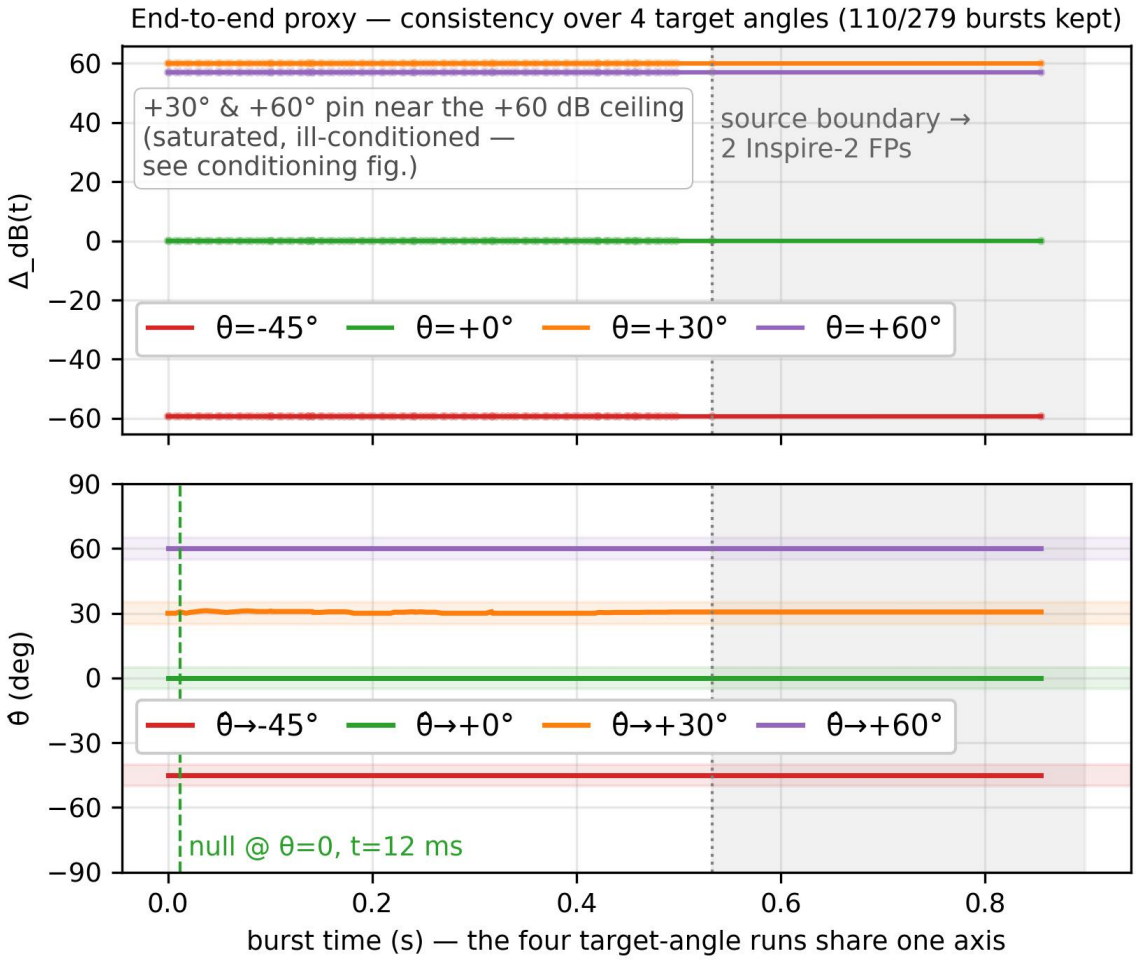
The end-to-end proxy processed 279 detected bursts and retained 110 at its configured fingerprint threshold (Fig. 2). The same retained burst set was evaluated under four simulated geometries, so 4/4 acceptance is one matched-model software-consistency exercise rather than four independent experiments. Two of the 110 retained bursts originated from the Inspire-2 control recording. Table 4 separates the null decision from its detection time and reports the corrected moving-block-bootstrap median interval.

An independent controlled acceptance sweeps at five angles and 25 dB signal-to-noise ratio yielded 5/5 within the 5° tolerance, with a maximum error of 0.70°. This verifies numerical behavior under the specified simulator; it is not an empirical field-accuracy estimate.

Table 4. **End-to-end direction-finding proxy results**

Angle	Kept	Median Δ_dB	MBB 95% CI	Estimated θ	Null?	Time
-45 degrees	110	-59.311 dB	[-59.3125, -59.3098] dB	-45.00 degrees	no	not applicable
+0 degrees	110	-0.001 dB	[-0.0020, -0.0003] dB	-0.00 degrees	yes	0.0117 s
+30 degrees	110	+59.999 dB	[+59.9963, +59.9996] dB	+30.60 degrees	no	not applicable
+60 degrees	110	+56.989 dB	[+56.9865, +56.9913] dB	+60.00 degrees	no	not applicable

Source: **compiled by the authors**



Bands are the ±5° acceptance windows (degrees).
2/110 kept bursts are Inspire-2 false positives (after the source boundary).

Fig. 2. **End-to-end proxy under four target angles (matched-model software-consistency view)**
Source: **compiled by the authors**

For the prototype geometry, the criterion-defined well-conditioned interval is open, approximately (−29.96°, +29.96°). The endpoints ±30° are excluded because one channel is saturated and the local differential slope is zero. At 0°, the slope is 0.455 dB/degree; the selected off-sector angles are also saturated and fail the combined slope-and-saturation criterion (Fig. 3 and Table 5).

Calibration model mismatch (Fig. 4) converts the matched-model identity into a sensitivity result. A 1 dB inter-channel gain imbalance produced a mean absolute error of 3.38° over the well-conditioned set and a maximum error of 60.40°. A 2° common boresight offset produced a 2.00° mean absolute bias. These curves are separate scenario sensitivities and are not summed.

Table 5. **Per-angle conditioning and multipath error**

θ	Conditioning	Two-ray median [95%]	Two-ray P(|e|>5°)	Rayleigh median [95%]; P(|e|>5°)
-45°	slope 0.094; saturated yes; W no	34.40 [0.65, 46.40]°	0.86	33.20 [18.66, 44.75]°; 1.00
+0°	slope 0.455; saturated no; W yes	8.30 [0.40, 11.28]°	0.73	3.40 [0.25, 9.21]°; 0.29
+30°	slope 0.000; saturated yes; W no	21.75 [0.00, 30.00]°	0.86	16.65 [6.50, 30.01]°; 0.99
+60°	slope 0.227; saturated yes; W no	53.65 [1.64, 66.35]°	0.85	51.25 [36.05, 64.83]°; 1.00

Source: **compiled by the authors**

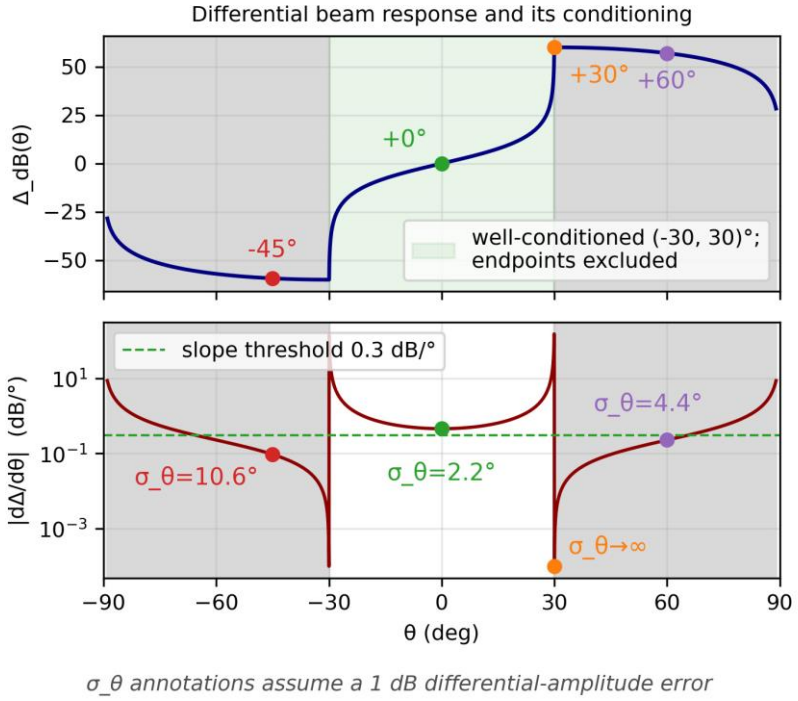


Fig. 3. **Differential response, local slope, saturation, and criterion-defined well-conditioned set**
Source: **compiled by the authors**

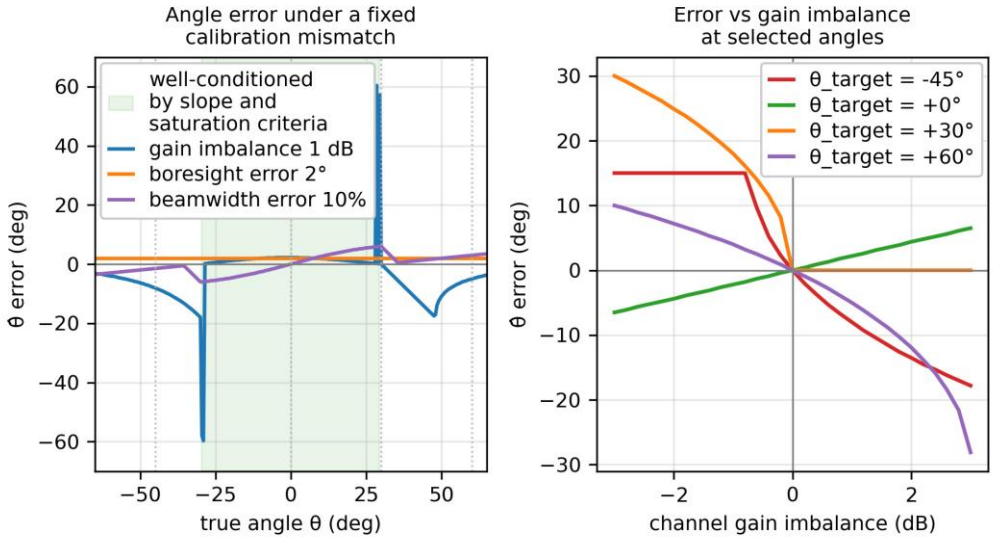


Fig. 4. **Angle error under antenna-calibration mismatch**
(left: vs angle at fixed mismatch; right: vs gain imbalance at the demo angles)
Source: **compiled by the authors**

The revised multipath analysis (Fig. 5) uses 100 independent nuisance realizations at each angle and relative-power level. At 0 dB multipath power, the median absolute error at 0° was 8.30° for the two-ray model and 3.40° for Rayleigh fading, with exceedance fractions 0.73 and 0.29. Saturated angles exhibit wide intervals and high exceedance fractions. The result is a Monte Carlo scenario distribution, not a field channel estimate.

Adjustment for a hypothetical target prior is illustrated in Fig. 6. The calculation propagates within-recording TPR/FPR and their uncertainty through Bayes' rule. Because the available negative class contains four controller recordings but no Wi-Fi, Bluetooth, or background/clutter captures, the curves are conditional transfer scenarios. No threshold is described as field-validated, and observed zero false positives on a finite sample is not treated as a field guarantee.

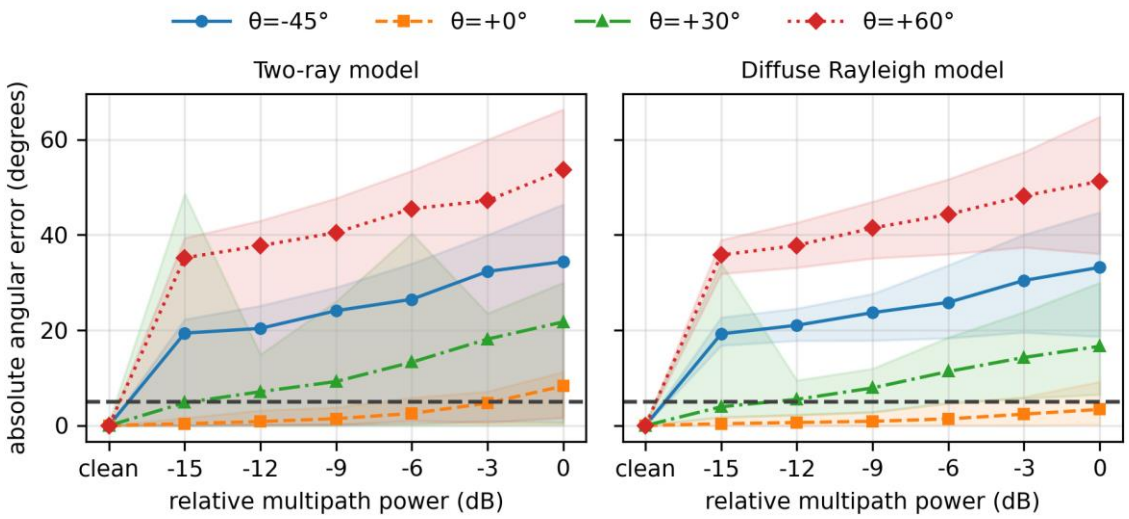


Fig. 5. **Monte Carlo multipath sensitivity: median absolute error and empirical 95% intervals**

Source: **compiled by the authors**

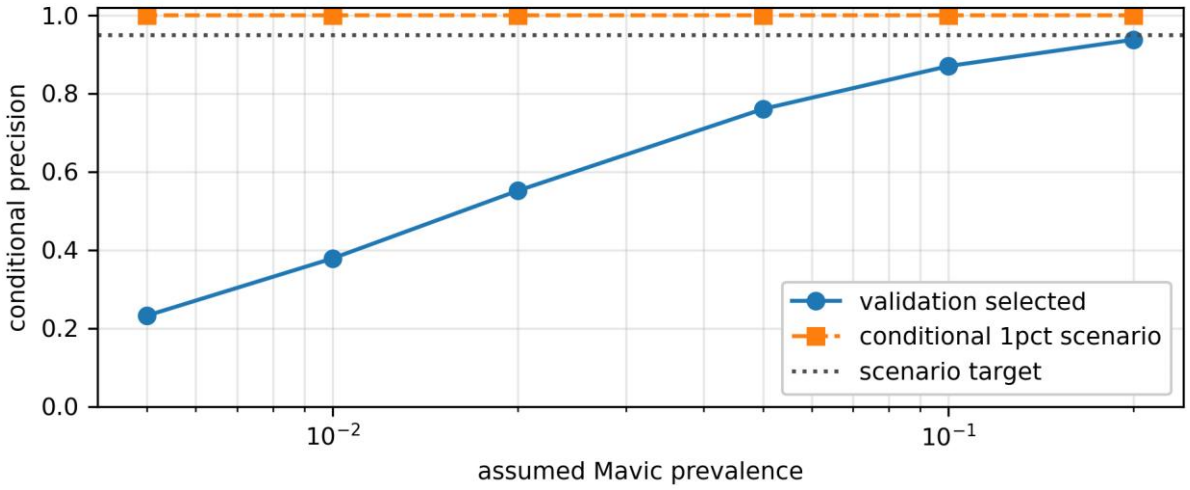


Fig. 6. **Conditional precision scenarios versus target prevalence using within-recording rates**

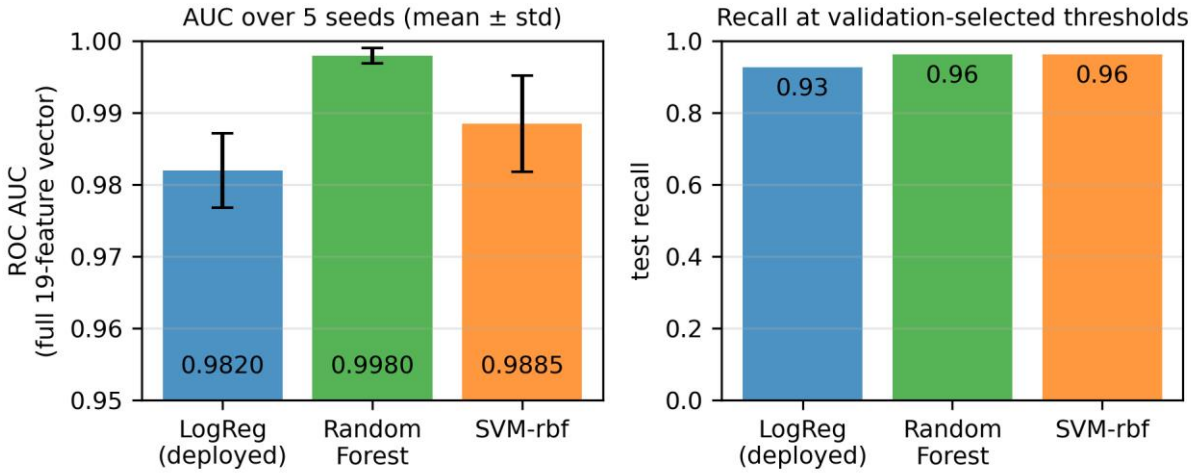
Source: **compiled by the authors**

Classifier sensitivity is reported in Table 6 and Fig. 7 using validation-selected thresholds. Across five seeds, mean ROC AUC was 0.9820 for logistic regression, 0.9980 for random forest, and 0.9885 for the radial-basis-function support-vector machine. On the untouched test block, recall was 0.9282, 0.9641, and 0.9641, respectively, while nonzero false-positive rates remained. These results show model sensitivity within the available recordings; they do not establish whether field performance is data-limited or model-limited.

Table 6. **Linear vs nonlinear fingerprint gate (same data pipeline)**

Gate	ROC AUC, mean ± SD (5 seeds)	Untouched-test recall; FPR	Conditional precision LCB at π=1 %
Logistic regression	0.9820 ± 0.0052	0.9282; 0.0154	0.2599
Random forest	0.9980 ± 0.0011	0.9641; 0.0141	0.2797
SVM–RBF	0.9885 ± 0.0067	0.9641; 0.0115	0.3090

Source: **compiled by the authors**



Within-recording blocks only; cross-device and field-clutter performance are untested.

Fig. 7. **Classifier sensitivity under validation-selected operating points and untouched-test evaluation**

Source: **compiled by the authors**

The end-to-end processing chain handled 279 detected bursts, retained 110, and completed in 26.7 s on the reported computer environment. The direction-finding values in Table 4 are matched-model consistency outputs; the empirical fingerprint metrics, conditioning mask, calibration perturbations, and Monte Carlo channel studies provide separate evidence relevant to applicability.

DISCUSSION OF RESULTS

The results should be interpreted on two levels. The consistency layer demonstrates that detected real bursts can pass through the fingerprint gate and the complete simulated dual-channel direction-finding chain. The sensitivity layer tests what that consistency does not prove: a threshold fixed before final evaluation, an interval aligned with the dependent median, geometric conditioning, calibration mismatch, multipath distributions, and negative-class coverage. The software checks therefore support implementation coherence, not cross-device or field accuracy.

The practical implications are direct. Operation should be confined to the criterion-defined unsaturated region, not to a closed ±30° sector. Calibration errors of approximately one decibel can produce several degrees of bias even in the well-conditioned set, and multipath can dominate the matched-model result. Fingerprint thresholds must be selected on validation data and re-evaluated against field-relevant interference rather than inferred from the available controller-only negatives.

The main limitations are one recording per controller class, no independent Mavic device or session, no Wi-Fi/Bluetooth/background negative mixture, simulated rather than measured dual-channel responses, and no independent antenna-pattern calibration. Field trials with a phase-coherent dual-channel receiver are planned. Their experimental design and results will be reported in a subsequent article.

Table 7. **Limitations and status**

Limitation	Status in this work	Required follow-up
Matched forward/inverse proxy	4/4 and 5/5 retained only as software-consistency checks	Calibrated hardware validation
Multipath absent from nominal proxy	100-draw two-ray and Rayleigh distributions reported separately	Field multipath measurements
Fingerprint prior and negative-class shift	Bayes curves are conditional; Wi-Fi/Bluetooth/background absent	Field-like negative sampling and recalibration
Open-data-only direction finding	Real single-channel I/Q; second channel simulated	Live phase-coherent dual-channel capture
One recording per device class	Within-recording held-out blocks only	Independent sessions and Mavic devices
No decoded OcuSync identifier	Plan-B physical-layer Fingerprint gate	separate protocol Study subject to legal and ethical constraints

Source: **compiled by the authors**

CONCLUSIONS

This study presents a reproducible integrated concept for amplitude-comparison direction finding

of DJI Mavic signals and reframes its evidence as model-based sensitivity analysis. The validation-selected fingerprint threshold produced precision 0.9378 and recall 0.9282 on an untouched within-recording test block, so the 0.95 precision criterion was not met. The moving-block-bootstrap interval now corresponds to the rolling median; ±30° are excluded from the well-conditioned set; and multipath is summarized over independent Monte Carlo realizations. The 4/4 proxy scenarios and 5/5 synthetic acceptance sweep remain software-consistency checks. Cross-device recognition, field-clutter rejection, calibrated dual-channel accuracy, and any joint error budget remain unverified.

Conflict of interests: Authors declare that they do not have conflict of interests, in particular financial, personal, copyright or any of a different nature, which could have influenced the research, as well as the results published in this article

Financing: Research was carried out without financial support

Accessibility data: The simulation code used to obtain given results, submitted in open repositories [https://github.com/SZabolotnii/SDR_POC_Pelengator-code-supplement]

Using artificial intelligence tools: During preparation manuscript used tool OpenAI Codex (GPT-5) and Claude Opus 5.5 of artificial intelligence (AI) for grammatical and stylistic text checks. All fragments processed by him were checked and edited by the author. AI was not used to generate text, formulas, and tables, formation scientific provisions, receipt results or formulation conclusions. Scientific the provisions, results and conclusions are my own, intellectual by the contribution of the authors

REFERENCES

1. Vuorenmaa, M., Marin, J., Heino, M., Turunen, M. & Riihonen, T. “Radio-frequency control and video signal recordings of drones”. *Zenodo*. 2020. DOI: https://doi.org/10.5281/zenodo.4264467.

2. Ezuma, M., Erden, F., Anjinappa, C. K., Ozdemir, O. & Guvenc, I. “Detection and classification of UAVs using RF fingerprints in the presence of Wi-Fi and bluetooth interference”. *IEEE Open Journal of the Communications Society*. 2020; 1: 60–76, https://www.scopus.com/pages/publications/85122046306. DOI: https://doi.org/10.1109/OJCOMS.2019.2955889.

3. Medaiyese, O. O., Ezuma, M., Lauf, A. P. & Adeniran, A. A. “Hierarchical learning framework for UAV detection and identification”. *IEEE Journal of Radio Frequency Identification*. 2022; 6: 176–188, https://www.scopus.com/pages/publications/85126283323. DOI: https://doi.org/10.1109/JRFID.2022.3157653.

4. Quadar, N., Chehri, A., Debaque, B., Yanikomeroglu, H. & Kurt, G. K. “Radio frequency fingerprinting: A survey of AI generalization challenges and solutions for wireless security”. *IEEE Open Journal of the Communications Society*. 2026; 7: 7587–7611. DOI: https://doi.org/10.1109/OJCOMS.2026.3701854.

5. Wong, L. J. & Michaels, A. J. “Transfer learning for radio frequency machine learning: A taxonomy and survey”. *Sensors*. 2022; 22 (4): 1416, https://www.scopus.com/pages/publications/85124358041. DOI: https://doi.org/10.3390/s22041416.

6. Jurn, Y. N., Ibraheem, Z. T. & Zaki, N. D. “A review of RF based drone detection, direction of arrival and identification techniques”. In *Proc. 2024 IEEE 14th International Conference on Control System, Computing and Engineering (ICCSCE)*. 2024. p. 162–167. DOI: https://doi.org/10.1109/ICCSCE61582.2024.10696847.

7. Flak, P. “Drone detection sensor with continuous 2.4 GHz ISM band coverage based on cost-effective SDR platform”. *IEEE Access*. 2021; 9: 114574–114586, https://www.scopus.com/pages/publications/85113316401. DOI: https://doi.org/10.1109/ACCESS.2021.3104738.

8. Kaplan, B., Kahraman, I., Ekti, A. R., Yarkan, S., Gorcin, A., Ozdemir, M. K. & Cirpan, H. A. “Detection, identification, and direction of arrival estimation of drone FHSS signals with uniform linear antenna array”. *IEEE Access*. 2021; 9: 152057–152069, https://www.scopus.com/pages/publications/85119397558. DOI: https://doi.org/10.1109/ACCESS.2021.3127199.

9. Liu, W., Haardt, M., Greco, M. S., Mecklenbräuker, C. F. & Willett, P. “Twenty-five years of sensor array and multichannel signal processing: A review of progress to date and potential research directions”. *IEEE Signal Processing Magazine*. 2023; 40 (4): 80–91. DOI: https://doi.org/10.1109/MSP.2023.3258060.

10. Richards, M. A. “Fundamentals of radar signal processing”. *3rd ed. McGraw-Hill*. 2022.

11. Hutar, M., Gil-Martínez, A., López-Pastor, J. A., Brida, P. & Gómez-Tornero, J. L. “Amplitude–monopulse design considerations for WiFi direction finding applications”. *IEEE Sensors Letters*. 2024; 8 (12): 1–4. DOI: https://doi.org/10.1109/LSENS.2024.3486343.

12. Ahmad, N., Nawaz, H., Shoaib, N., Abbasi, Q. H. & Nikolaou, S. “Ambiguity resolution in amplitude-comparison-based monopulse direction-finding antenna systems”. *IEEE Antennas and Wireless Propagation Letters*. 2023; 22 (10): 2605–2609, https://www.scopus.com/pages/publications/85165915905. DOI: https://doi.org/10.1109/LAWP.2023.3298664.

13. Han, S. & Jang, B.-J. “Drone’s angle-of-arrival estimation using a switched-beam antenna and single-channel receiver”. *Sensors*. 2025; 25 (8): 2376. DOI: https://doi.org/10.3390/s25082376.

14. Wang, X., Yan, X., An, T., Chen, Q. & Huang, D. “Underdetermined direction of arrival estimation with nonuniform linear motion sampling based on a small unmanned aerial vehicle platform”. *Defence Technology*. 2024; 33: 352–363, https://www.scopus.com/pages/publications/85164397552. DOI: https://doi.org/10.1016/j.dt.2023.06.006.

15. Almasri, S. A., Johannsen, N. L. & Hoeher, P. A. “Direction-of-arrival estimation for unmanned aerial vehicles and aircraft transponders using a multi-mode multi-port antenna”. *Sensors*. 2024; 24 (11): 3452, https://www.scopus.com/pages/publications/85195982885. DOI: https://doi.org/10.3390/s24113452.

16. Künsch, H. R. “The Jackknife and the Bootstrap for general stationary observations”. *Annals of Statistics*. 1989; 17 (3): 1217–1241. DOI: https://doi.org/10.1214/aos/1176347265.

17. Rappaport, T. S. “Wireless communications: Principles and practice”. *2nd ed. Prentice Hall*.

18. Kunchenko, Y. P. “Approximation polynomials in a space with generating element”. *Naukova Dumka*. 2003.

19. Zabolotnii, S. V., Chepynoha, A. V. & Hotunov, V. I. “From statistical pattern recognition to emotion analysis: Application of decomposition in a space with a generating element for NLP models”. *Cybernetics and Systems Analysis*. 2026; 62 (2): 325–334, https://www.scopus.com/pages/publications/105037331212. DOI: https://doi.org/10.1007/s10559-026-00870-7.

20. Zabolotnii, S. “Applying the polynomial maximization method to estimate ARIMA models with asymmetric non-gaussian innovations”. *arXiv*. 2025. DOI: https://doi.org/10.48550/arXiv.2511.07059.

21. Zabolotnii, S. “Parametrically adaptive transition polynomial: a signed-parity continuous-alpha extension of Kunchenko stochastic polynomials”. *arXiv*. 2026. DOI: https://doi.org/10.48550/arXiv.2605.14610.

Received 26.08.2026
Received after revision 19.10.2026
Accepted 30.10.2026

DOI: https://doi.org/10.15276/hait.09.2026.41
УДК 621.396.67:621.391:004.89

Модельний аналіз чутливості двоканальної пеленгації сигналів керування безпілотних літальних апаратів засобами програмно визначуваного радіо

Заболотній Сергій Васильович[1), 3)]
ORCID: https://orcid.org/0000-0003-0242-2234; zabolotnii.serhii@csbc.edu.ua. Scopus Author ID: 56352587900
Чепинога Анатолій Володимирович[2)]
ORCID: https://orcid.org/0000-0003-3921-6557; a.chepynoha@chdtu.edu.ua. Scopus Author ID: 57222273315
Коваль Віталій Володимирович[3)]
ORCID: https://orcid.org/0000-0003-0158-4872; vitkoval@ukr.net
Клопотовський Павло Анатолійович[2)]
ORCID: https://orcid.org/0000-0002-4958-2377; p.klopotovskyi@chdtu.edu.ua. Scopus Author ID: 60633744900
[1)] Черкаський державний бізнес-коледж, вул. Чорновола, 243. Черкаси, 18028, Україна
2) Черкаський державний технологічний університет, бульв. Шевченка, 460, Черкаси, 18006, Україна
3) Державний науково-дослідний інститут випробувань і сертифікації озброєння та військової техніки, Черкаси, Україна

АНОТАЦІЯ

Актуальність. Пеленгація випромінювань каналів керування безпілотниками є важливою для радіочастотного моніторингу, однак відкриті дані не містять когерентних двоканальних записів і незалежних екземплярів пристроїв. **Мета.** Перевірити внутрішню узгодженість відтворюваного конвеєра з радіочастотним фільтром та амплітудно-порівняльною пеленгацією за заданої моделі антени й визначити межі застосування. **Завдання.** Розділити налаштування та остаточне оцінювання, узгодити інтервал невизначеності з медіаною, дослідити обумовленість, калібрування, багатопроменевість і склад негативного класу без необґрунтованого сумарного бюджету похибок. **Методи.** Одноканальні записи Тампере, представлені синфазною та квадратурною складовими, використовуються для виявлення пакетних сигналів і формування їхніх радіочастотних відбитків; другий канал і діаграми спрямованості антен моделюються штучно. Повні записи хронологічно розподіляються на навчальну, валідаційну та тестову вибірки, які розмежовуються захисними часовими інтервалами. Порогове значення обирається виключно за валідаційними даними. Використано довірчі інтервали Вілсона, а площа під кривою робочих характеристик приймача оцінюється методом стратифікованого бутстрепу. Для нульового детектора довірчий інтервал медіани визначається методом кругового рухомого блочного бутстрепу. Чутливість до багатопроменевості підсумовується за незалежними вибірками перешкод у кожній точці моделі. **Наукова новизна.** Внеском є відтворювана інтеграція з перевірюваними межами: добре обумовлена множина потребує достатнього нахилу кривої диференціальної реакції й відсутності насичення, а твердження про ідентифікацію обмежено покриттям записів і негативних класів. **Практична значущість.** Процедура усуває вибір порога на тесті й задає перевірки геометрії та калібрування перед апаратними випробуваннями. **Результати.** Вибраний на валідації поріг забезпечив на недоторканому тестовому блоці високі влучність і повноту, проте заздалегідь заданий критерій влучності не виконано. Крайні кути сектора вилучено з добре обумовленої множини через насичення одного з каналів і зникнення локального нахилу. **Висновки.** Конвеєр обчислювально узгоджений у межах моделі, але міжплатформне розпізнавання, робота на тлі польових завад і калібрована двоканальна точність не перевірені.

Ключові слова: програмно визначуване радіо; пеленгація; радіочастотна ідентифікація; амплітудне порівняння; бутстреп залежних даних; безпілотна авіаційна система

ABOUT THE AUTHORS



Serhii V. Zabolotnii - Doctor of Engineering Sciences, Professor, Department of Computer Engineering and Information Technologies. Cherkasy State Business College, 243, Chornovola Str. Cherkasy, 18028, Ukraine
ORCID: https://orcid.org/0000-0003-0242-2234; zabolotnii.serhii@csbc.edu.ua. Scopus Author ID: 56352587900
Research field: artificial intelligence, machine learning, natural language processing, signal processing, non-Gaussian statistical estimation, software-defined radio

Заболотній Сергій Васильович - доктор технічних наук, професор кафедри Комп'ютерної інженерії та інформаційних технологій. Черкаський державний бізнес-коледж, вул. Чорновола, 243. Черкаси, 18028, Україна
Галузь досліджень: штучний інтелект, машинне навчання, обробка природної мови, обробка сигналів, негаусове статистичне оцінювання, програмно-кероване радіо



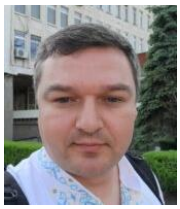
Anatolii V. Chepynoha - Candidate of Engineering Sciences, Associate Professor, Dean of Faculty of Information Technologies and Systems. Cherkasy State Technological University, 460, Shevchenka Bulv. Cherkasy, 18006, Ukraine
ORCID: https://orcid.org/0000-0003-3921-6557; a.chepynoha@chdtu.edu.ua. Scopus Author ID: 57222273315
Research field: signal processing, non-Gaussian statistical estimation, software-defined radio, cybersecurity

Чепинога Анатолій Володимирович - кандидат технічних наук, доцент, декан факультету Інформаційних технологій і систем. Черкаський державний технологічний університет, бульв. Шевченка, 460. Черкаси, 18006, Україна
Галузь досліджень: обробка сигналів, негаусове статистичне оцінювання, програмно-кероване радіо, кібербезпека



Vitalii V. Koval - Candidate of Engineering Sciences, Associate Professor, Research Scientist State Scientific Research Institute of Armament and Military Equipment Testing and Certification, Cherkasy, Ukraine
ORCID: https://orcid.org/0000-0003-0158-4872; vitkoval@ukr.net
Research field: polynomial models and methods, software-defined radio

Коваль Віталій Володимирович - кандидат технічних наук, доцент, науковий співробітник Державного науково-дослідного інституту випробувань і сертифікації озброєння та військової техніки, Черкаси, Україна
Галузь досліджень: поліноміальні моделі та методи, програмно-кероване радіо



Pavlo A. Klopotovskyi - Senior Lecturer, Department of Robotics and Telecommunications Systems and Cybersecurity. Cherkasy State Technological University, 460, Shevchenka Bulv. Cherkasy, 18006, Ukraine
ORCID: https://orcid.org/0000-0002-4958-2377; p.klopotovskyi@chdtu.edu.ua. Scopus Author ID: 60633744900
Research field: artificial intelligence, signal processing, non-Gaussian statistical estimation, and software-defined radio

Клопотовський Павло Анатолійович - старший викладач кафедри Робототехнічних і телекомунікаційних систем та кібербезпеки. Черкаський державний технологічний університет, бульв. Шевченка, 460. Черкаси, 18006, Україна
Галузь досліджень: штучний інтелект, обробка сигналів, негаусове статистичне оцінювання та програмно-кероване радіо